PHYSICAL REVIEW D **83,** 062004 (2011)

SGR 1806-20 and the gravitational wave detectors EXPLORER and NAUTILUS

G. Modestino* and G. Pizzella†

INFN, Laboratori Nazionali di Frascati, I-00044, Frascati (Roma) Italy

(Received 6 May 2010; revised manuscript received 21 October 2010; published 16 March 2011; corrected 12 April 2011)

The activity of the soft gamma ray repeater SGR 1806-20 is studied in correlation with the EXPLORER and NAUTILUS data, during the year 2004, for gravitational wave (GW) short signal search. Corresponding to the most significant triggers, the bright outburst on October 5th and the giant flare (GF) on December 27th, the associated GW signature is searched. Two methods are employed for processing the data. With the average-modulus algorithm, the presence of short pulses with energy $E_{gw} \geq 1.8 \times 10^{49}$ erg is excluded with 90% probability, under the hypothesis of isotropic emission. This value is comparable to the upper limits obtained by LIGO regarding similar sources. Using the cross-correlation method, we find a discrepancy from the null-hypothesis of the order of 1%. This statistical excess is not sufficient to claim a systematic association between the gravitational and the electromagnetic radiations, because the estimated GW upper limits are yet several orders of magnitude far away from the theoretically predicted levels, at least three for the most powerful SGR flare.

DOI: 10.1103/PhysRevD.83.062004 PACS numbers: 04.80.Nn, 95.55.Ym, 95.85.Sz

I. INTRODUCTION

Discovered since 1979 [1,2], despite their unpredictable behavior, the soft gamma repeaters (SGRs) are considered interesting targets in gravitational wave (GW) studies. The fundamental ideas are the neutron star nature of these objects and the association of SGRs with magnetars [3,4]. Detected as persistent x-ray source at $\sim 10^{35}$ ergs s^{-1}, they occasionally emit energetic soft gamma bursts, up to $\sim 10^{42}$ ergs s^{-1}, or even much more energetic events. The large number of observed characteristics of SGRs, including the bursting activity during the three giant flares (GFs) detected to date [1,5–7], confirm the neutron star nature of SGR, and offer an effective evidence of the presence of very high magnetic field ($B \sim 10^{15}$ G). (For a review, see [8]). According to several models, the burst triggers are primary reference studying the gravitational radiation [9–13]. The most optimistic GW emission model [10] foresees an extreme bursting activity, probably due to a sudden global reconfiguration of the internal magnetic field, and the magnetar shape deformation, causing the increase in the momentum of inertia with a release of energy through gravitational radiation. Also, the proximity (~ 10 kpc) makes these objects intriguing for GW searches, enhancing chances of detectability.

To this aim, several measurements had previously been performed. Studying the GF occurring on December 27th 2004, the AURIGA group [14] explored the frequency range 930–935 Hz, under the hypothesis of oscillating emission with a damping time of 100 ms. Expressing the result in terms of the dimensionless amplitude h, they found an upper limit of 2.7×10^{-20}, at the time of the hyperflare. In relation to the same event, the LIGO collaboration [15] examined the pulsating tail of the burst which revealed the presence of quasiperiodic oscillations in the x-ray light curve, as RXTE and RHESSI satellite had detected [16,17]. LIGO found no excess and, racing from $\sim 10^{47}$ ergs, they set several upper limit levels on the GW emitted energy, depending on time and frequency radiation. More recently, the same LIGO collaboration presented the results of short-duration GW events associated with SGR 1806-20 and SGR 1900+14 storms occurred during the year starting from November 2005 [18–20]. Including the GF on December 27th, they analyzed almost 200 events, finding no evidence of any association. Depending on signal waveform types, several upper limits are estimated, referring to more than five orders of the GW energy magnitude (from 10^{45} erg to almost 10^{51} erg) for hypothetical isotropic GW emission.

In the present paper, we consider the particular phenomenon of the SGR 1806-20 during the year 2004. The resonant GW detectors EXPLORER and NAUTILUS [21] data are analyzed corresponding to the long sequence that occurred on October 5th [22], and to the GF on December 27th. As previously seen, during this event, several observations were performed using GW experimental apparatuses but, as far as the October outburst is concerned, there were no previous GW measurements although it represents a very significant event because of the exceptional energy release and duration, extending 3×10^{42} erg over more than 100 pulses in a 10-minute span of time.

The principal points of the present analysis are as follows. The presence of short pulses (up to a few tenths of a millisecond) was searched for on both GW detectors, using the data filtered by a linear filter matched to δ-like signals. In Sec. II, the sensitivity of the apparatuses is shown relatively to the year 2004. As explained in Sec. III A, the physical regions were chosen on two long sequences of 26s plus 46s , corresponding to the highest electromagnetic

*giuseppina.modestino@lnf.infn.it
†guido.pizzella@lnf.infn.it

(EM) peaks of the October 5th outburst, and on 1s centered around the trigger time of the GF on December 27th. The long period, in the case of the outburst, and knowledge of the arrival time on Earth of a light-speed signal at the time of the GF [7,14] are circumstances particularly opportune to avoid uncertainty in the analysis focusing on the reference time of the gravitational radiation. The expected distribution under the null-hypothesis is built using real data, with random time shifts of one GW detector with respect to the other one (Sec. III B). Essentially, two algorithms are employed. With the first, discussed in Sec. IV, we evaluate the excess amplitude on the on-source regions of the GW detector data. With this measurement (calibrated using the cosmic ray signals [23], as explained in the Appendix), we exclude the presence of the GW short signal and we establish the upper limit to the amount of isotropic GW energy E_{GW} emitted during the exceptional periods. The second algorithm regards the cross-correlation function calculated between the EXPLORER and NAUTILUS data streams, as shown in Sec. V. Following previous methods [24–27], cumulative analyses are performed on the sample of 73 measurements, obtaining several mismatches of the order of 1% probability or less from the background. The statistical significance is evaluated on the basis of the local probability and binomial tests of the resulting loudest measurements. In the final discussion, Sec. VI, we provide a summary of the study and further comments.

II. EXPLORER AND NAUTILUS SENSITIVITY

We consider the EXPLORER and NAUTILUS operating during 2004 [21], using the filtered data setup as the ROG collaboration released [28]. The main characteristics of the experimental apparatuses, in terms of frequency coverage, are shown in Table I. The frequency region where the detectors are sensitive covers a range of about 100 hertz, thanks to which the data can be sampled at time intervals of 3.2 ms. The data are filtered with a filter matched to delta-like signals for the detection of short bursts [29], typically of the order of a few milliseconds.

Let $x(t)$ be the filtered output of the detector. For well-behaved noise due to the thermal motion of the oscillators and to the electronic noise of the amplifier, the distribution of $x(t)$ is normal with zero mean. Its variance represents the *effective temperature* and is indicated with T_{eff}. The distribution of $x(t)$ is

$$f(x) = \frac{1}{\sqrt{2\pi T_{\mathrm{eff}}}} e^{-((x^2)/(2T_{\mathrm{eff}}))}. \tag{1}$$

During the year 2004, T_{eff} was 2.0 mK for EXPLORER and 1.7 mK for NAUTILUS.

The resonant detectors are able to measure the Fourier component H of the incoming gravitational radiation with dimensionless amplitude $h(t)$. The apparatuses' sensitivity (SNR = 1) to short burst can be expressed as the minimum detectable H [30,31]

$$H_{\mathrm{min}} = \frac{1}{4Lf_0^2}\sqrt{\frac{k_B T_{\mathrm{eff}}}{M}}\left[\frac{1}{\mathrm{Hz}}\right], \tag{2}$$

where k_B is the Boltzmann constant and f_0, L and M are the resonance frequency, the length and the mass of the bar. In general, if we detect a burst with energy E_s, expressed in kelvin units, the corresponding value is

$$H = \frac{1}{4Lf_0^2}\sqrt{\frac{k_B E_s}{M}} \simeq 2.4 \times 10^{-22}\sqrt{E_s\ (\mathrm{mK})}\left[\frac{1}{\mathrm{Hz}}\right] \tag{3}$$

for optimal orientation.

Besides the single bursts, this search is suitable for any GW transient which shows a nearly flat Fourier spectrum at the two resonant frequencies of each detector. The metric perturbation $h(t)$ can either be a millisecond pulse, a signal made by a few millisecond cycles, or a damped sinusoid signal. In the hypothesis of a signal sweeping in frequency through the detector resonances, with small decay times (< 50 ms), the filter maintains good detection capability [32–34]. For a short signal of duration time τ_g and frequency $f_g \sim f_0$, the spectral amplitude, $\tilde{h} = \sqrt{\int |H(f)|^2 df}$, can be put

$$\tilde{h} \simeq H\sqrt{\pi/\tau_g}\left[\sqrt{\frac{1}{\mathrm{Hz}}}\right]. \tag{4}$$

III. DATA SELECTION

During the year 2004, several detectors on spacecraft observed a special activity from SGR 1806-20 culminating on December 27th. Before the GF, other considerable events occurred, such as the strong outburst October 5th, when more than 100 short bursts were emitted in a few minutes, involving more than 3×10^{42} erg in terms of EM energy release [22]. In the last reference, there is an

TABLE I. Resonant frequencies of EXPLORER and NAUTILUS during 2004, instrumental bandwidth Δf and relative sensitivities.

detector	resonances f [Hz]	Δf [Hz]	H_{min} $[\frac{1}{\mathrm{Hz}}]$
EXPLORER	904.7, 921.3	8.7	3.4×10^{-22}
NAUTILUS	926.3, 941.5	9.6	3.1×10^{-22}

accurate description of the event and relative light curves of the initial brighter part. The instruments (in the 15–200 keV energy range) indicate two very intense peak clusters, the first one in the vicinity of the trigger at 13:56:49 UT, the second one after about three minutes.

A. On-source region

Referring to the cited EM triggers, we consider physically interesting the following time periods of the filtered data of both EXPLORER and NAUTILUS:

(a) on October 5th, 13:56:44–13:57:10, 26s (starting 5s before the EM trigger);
(b) on October 5th, 13:59:39–14:00:25, 46s during the second cluster of bright bursts;
(c) on December 27th, 21:30:26.14–21:30:27.14, 1s centered to the GF trigger time [6,7].

The choice of the two long first periods is due to the special profile of the light curves, but it is also opportune to avoid any uncertainty about the time delay between the two emissions that make the time reference definition difficult in the correlation study. Nevertheless, relative to the GF, it is possible to restrict the measurement period because the impinging time of a light-speed signal onto the GW detectors is known [14]. Since the three different lengths (26s, 46s, 1s) do not allow us to employ an easy algorithm for a uniform analysis from the statistical and physical point of view, we divide the two long periods into a number of contiguous intervals, 1s for each one, obtaining a comprehensive sample of 73 independent segments for performing measurements. We call the GW detector data in this region on-source data. All routine checks are done on the selected period, principally by vetoing with a threshold on $T_{\rm eff}$, to ensure good sensitivity and stationary data. In addition, we also control the presence of local noise anomalies, and the effectiveness of the division into 1s segments, evaluating the autocorrelation function to the EXPLORER and NAUTILUS data of the on-source a and b periods, as explained in the Appendix.

B. The background data

For estimating the expected result under the null-hypothesis, we use real data but considering time regions distant a few hours away the EM triggers. By assigning 3000 random time steps, we obtain as many off-source 1s segments for the first GW detector. To avoid simultaneous signals of any nature, we apply a time shift of several hours on the data sequence of second GW detector with the respect the first one, thereby obtaining as many as 3000 off-source segments. All periods are selected vetoing by a threshold on $T_{\rm eff}$, consistently with the on-source region selection.

IV. THE AVERAGE ALGORITHM

The first algorithm for scanning the on-source data is designed to detect an enhancement due to a GW burst. Because of the oscillating character of the response, we average over 1s the amplitude modulus of each sample, x_i for EXPLORER and y_i for NAUTILUS, belonging to the on-source segments. The averaged signal parameter is indicated with

$$AS \equiv \frac{\Sigma_{i=1}^{n}|x_i| + \Sigma_{i=1}^{n}|y_i|}{2n}[\sqrt{K}], \tag{5}$$

where $n = 313$, the number of 3.2 ms samples in each second. Applying the Eq. (5) to the 73 pairs on-source segments, we obtain the distribution in Fig. 1. The relative background, the lightest area of Fig. 1, is calculated on the 3000x2 segments that have been previously defined. Cumulative calculations give: $\bar{AS}_{73} = 3.29 \times 10^{-2}\sqrt{K}$, very close to the $AS_{\rm bck}$ value (3.28×10^{-2}, with root-mean-squared, RMS $= 2.8 \times 10^{-3}\sqrt{K}$). Comparing the distributions by the Kolmogoroff test, we obtain 45% probability that the AS measured distribution is similar to the background one. The high compatibility value and, as we can easily note, the absence of loud events in the distribution, clearly indicate that no amplitude excess is present on the physical region. Thus, we do not retain to perform further statistical investigation on this result. Rather, considering the particular phenomenon and the experimental calibration by the cosmic ray excitation, this measure assumes an important significance in terms of upper limit for energy evaluation of emitted gravitational radiation.

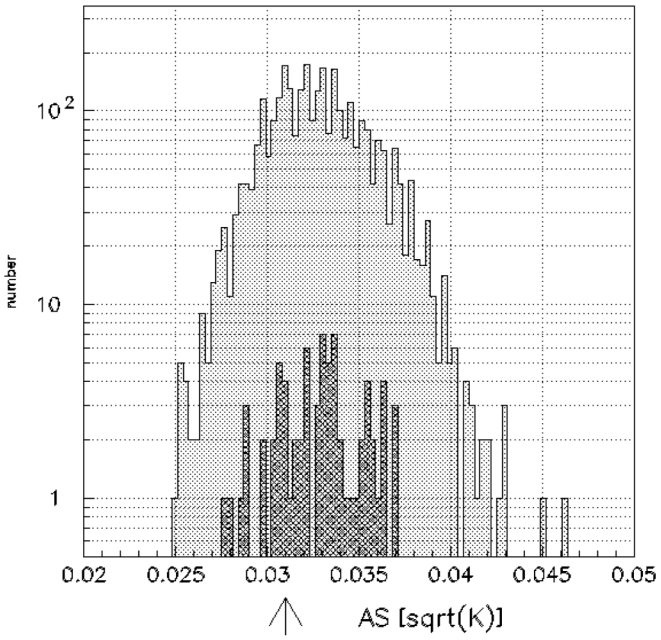

FIG. 1. Distribution of the 73 AS parameter values (the darkest area), as defined in Sec. IV. The lightest part is the background distribution of the same parameter evaluated on the off-source regions. The Kolmogoroff compatibility test gives 45% probability. The arrows indicates the AS evaluation on the data streams at the time of the GF.

TABLE II. Upper limits for gravitational waves with the EXPLORER and NAUTILUS detectors, using the AS quantity.

2004 day	period length (s)	AS $[\sqrt{K}]$	$\tilde{h}^{90\%}$ $[\frac{1}{\sqrt{\text{Hz}}}]$	$E_{\text{GW}}^{90\%}$ [erg]	EM [erg]
1) Oct 5th	26 + 46	$3.29 \times 10^{-2} \pm 0.3 \times 10^{-3}$	2.9×10^{-21}	1.8×10^{49}	3×10^{42}
2) Dec 27th	1	$3.11 \times 10^{-2} \pm 0.28 \times 10^{-2}$	4.3×10^{-21}	4×10^{49}	1.6×10^{46}

A. Upper limit

In the present study, two different levels are present in terms of source type. 1) Several peaks belonging to the outburst on October 5th, when the EM energy release of 3×10^{42} erg was involved. 2) The GF with 1.6×10^{46} erg of isotropic E_{EM} in the main peak [7]. There are 4 orders of magnitude in terms of emitted energy between them, so we need to distinguish two measurement levels. In Table II, corresponding to each category, we set out the AS measured parameter. By the cosmic ray calibration procedure, as explained in the Appendix, the input signal energy values are extracted. From the Eqs. (3) and (4), assuming an incoming burst with duration time τ_g and $f \sim f_0$, the spectral amplitudes $\tilde{h}$ are evaluated. Under the frequentist approach [35], the relative upper limits are calculated, at 90% confidence level, setting $\tilde{h} = 2.9 \times 10^{-21}\sqrt{1/\text{Hz}}$, for the period 1), and $\tilde{h} = 4.3 \times 10^{-21}\sqrt{1/\text{Hz}}$, for the period 2).

Using the classical resonant detector cross section, under the hypothesis of isotropic emission, the total energy carried by the gravitational waves is given by

$$E_{\text{GW}} = \frac{\pi^2 c^3}{8G} \frac{1}{ML^2 f^2} \frac{r^2}{\tau_g} E_s = 37.4 \times 10^{49} \frac{1\ \text{ms}}{\tau_g} \left(\frac{r}{10\ \text{kpc}}\right)^2 E_s\ (\text{mK})\,[\text{erg}], \quad (6)$$

where r is the source distance, τ_g is the signal duration and E_s expressed in mK units. For the categories in Table II, under the hypotheses of an isotropic emission, the corresponding E_{GW} upper limits are 1.8×10^{49} erg and 4×10^{49} erg, with duration time $\tau_g = 30$ ms and $r = 10$ kpc. In order to compare the results to previous similar measurements, we need to consider the ratio $\gamma = \frac{E_{\text{GW}}}{E_{\text{EM}}}$. The importance of this parameter is well-pointed in a series of LIGO analyses regarding the association with SGRs [18–20]. Their results are distributed over a wide interval comprising almost 8 orders of magnitude in terms of γ, depending on several signal waveform hypotheses and on relative sensitivities. In our measurements, $\gamma^{90\%} = 6 \times 10^6$, for October outburst, and $\gamma^{90\%} = 2.5 \times 10^3$, for the December GF. These values are included in the ranges established by previous cited measurements.

V. THE CROSS-CORRELATION RESPONSE

We correlate the data of EXPLORER and NAUTILUS processed with the filter matched to deltalike signals by taking simultaneous time periods of data of both detectors lasting 1s each (on-source regions), calculating the cross-correlation function

$$r(\tau) = \frac{\varepsilon[(x(t+\tau) - \bar{x})(y(t+\tau) - \bar{y})]}{\sqrt{\varepsilon[(x(t) - \bar{x})^2 \varepsilon[(y(t) - \bar{y})^2]}} \quad (7)$$

where the filtered data of EXPLORER are indicated with $x(t)$, and the filtered data of NAUTILUS, with $y(t)$. $\bar{x}$ is the average value of x, $\bar{y}$ that of y and $\varepsilon[\ldots]$ is the *expectation*. We consider the maximum value of the correlation function

$$r_{\text{max}} \equiv \max r(\tau) \qquad \tau \in [-16\ \text{ms}, 16\ \text{ms}]. \quad (8)$$

In this way, we take care of possible small time mismatches between the two detectors and also of the fact that the real excitation may not be properly shaped with the

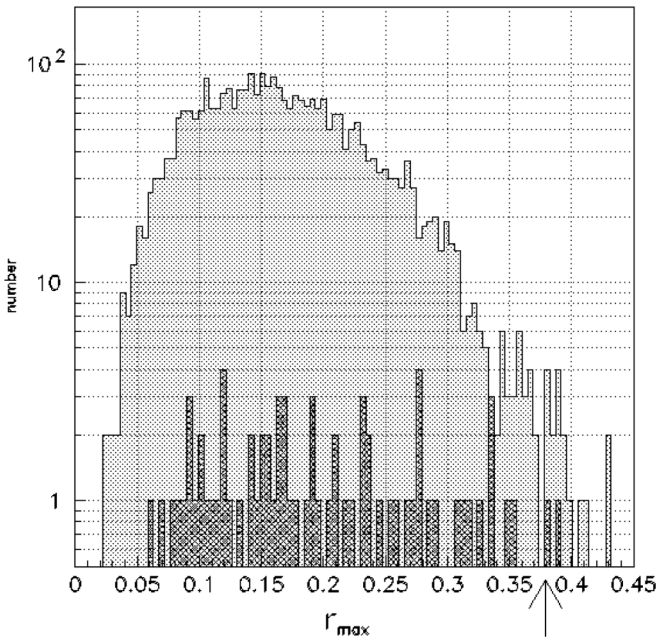

FIG. 2. Distribution of r_{max}, the maximum value of the cross-correlation function for $\tau = \pm 16$ ms, evaluated on the 73 on-source regions (the darkest area). The lightest part is the distribution of the same parameter evaluated on the background 3000 off-source regions. The Kolmogoroff compatibility test gives 1.3% probability. The arrows indicates the value at the time of GF.

delta-function used in the matched filter. (In the Appendix, we show how this procedure is applied to data which include cosmic ray excitations.) The distribution of the 73 $r_{\max}$ values is shown in Fig. 2 with the relative background. Also, for $r_{\max}$ the expected distribution under the null-hypothesis is empirically evaluated using the 3000 pair stretches built as described in Sec. III B. The comparison by Kolmogoroff test gives 1.3% of probability that the two distributions are similar.

Statistical tests

Considering that a GW signal from individual 1s time periods could likely be weak, we test for a cumulative signature associated with the whole segment sample. In the past, this method has been applied to study correlations between EXPLORER and NAUTILUS data and gamma-ray bursts [24,25]. It has been also used and developed in the second, third and fourth LIGO science run data analysis [26], and more recently, in the enlarged LIGO-Virgo collaboration for gamma-ray burst search [27]. In the last cited papers, we find especially useful the probability distribution study and the binomial test, in order to better appraise the statistical significance of the loudest correlations and to select candidate events. In our case, the same method can be helpful to mark time segments that particularly deviate from the background. The cumulative local probability distribution (Fig. 3) is associated to the $r_{\max}$ measurements. The tail of the p local distribution corresponds to the loudest $r_{\max}$ values. In the same figure, the expected distribution under the null hypothesis is indicated by the solid line. As easily noted, the p tail shows an extended deviation from the background. Corresponding to the measurements with local probability $p \leq 0.1$, we calculate the binomial probabilities $P_{\geq i}(p_i)$ of getting i or more events with $p \leq p_i$, obtaining a spectrum which ranges down to 5.5×10^{-6} (at $p_{18} = 0.075$). The measurement relative to the GF segment gives the second largest $r_{\max}$ value, setting $p_2 = 7 \times 10^{-3}$, and $P_{\geq 2} = 0.093$. We perform further statistical investigations taking into account unforeseeable nonstationary effects in the data, and the empirical form of the employed algorithm. Sorting $k = 20000$ different arrangements, composing each one with 73 random draws from the null-hypothesis distribution of Fig. 2, we estimate the binomial value $P_{\geq i}(p_i, k)$, and the minimum $P(k)_{\min}$, between the 73 values of the kth set. Comparing it with the real best result, we count how many times $P(k)_{\min} \leq 5.5 \times 10^{-6}$. It happens 2 times out of the 20000 different arrangements. We also calculate the expected number of events for having a 1% confidence excess with respect to the null hypothesis, at given probabilities $p \leq 0.1$. These values are shown in Fig. 3 with the dashed line. From the comparison with the $r_{\max}$ on-source distribution (the bullets in the same figure), we note a discrepancy with the null hypothesis with probabilities well below 1%, in the region $0.02 \leq p \leq 0.1$.

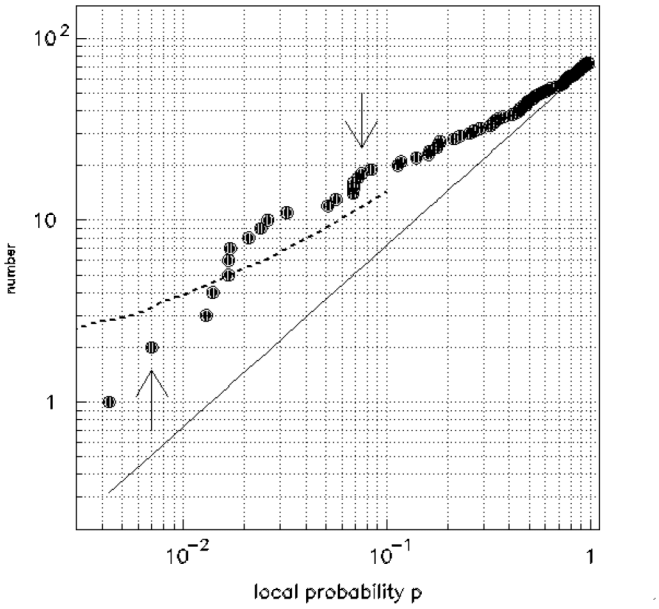

FIG. 3. The cumulative local probability p distribution for $r_{\max}$ parameter. The 73 on-source measurements are represented by the bullets. The continuous line is the null-hypothesis $r_{\max}$ distribution normalized to the number of measurements. The dashed line gives the excess needed for a 1% confidence level in the null hypothesis. The up-arrow indicates the local probability level of $r_{\max}$ at the time of the GF. The down-arrow points to the best real result in terms of binomial probability $P_{\geq 18}(0.075) = 5.5 \times 10^{-6}$.

VI. DISCUSSION

We studied the EXPLORER and NAUTILUS data in correlation with the astrophysical gamma-ray bursts during the year 2004, when an exceptional activity was observed in terms of electromagnetic emission. In particular, we examined the long outburst that occurred on October 5th, considering the two time intervals containing the major peaks, (respectively of 26s and 46s), and 1s time intervals centered on the outstanding flare on December 27th. On the resulting sample of 73 segments in total, 1s each one, we employed two algorithms. The first one consists in averaging the absolute values of the EXPLORER and NAUTILUS responses on the on-source region, and calibrating with the transfer function of real delta signals due to the cosmic ray excitations. Assuming the hypothesis of GW short pulses, no significant excess is found either with the overall statistic sample, or by analyzing the segments with loudest amplitude values. We obtain the upper limit expressed as amplitude signal or GW energy released by the astrophysical source with respect to two energy ranges. Considering the bright outburst of October, involving a release of $\sim 10^{42}$ erg, the result is $E_{\mathrm{GW}}^{90\%} = 1.8 \times 10^{49}$ erg. With regard to the GF, when an isotropic electromagnetic energy of 1.6×10^{46} erg is assumed, the upper limit is 4×10^{49} erg. They are comparable with

previous values obtained by LIGO, in the frequency band 100–1000 Hz.

We also processed the EXPLORER and NAUTILUS data, on the same on-source segments, using the cross-correlation algorithm and applying a series of statistical tests. This analysis shows a compatibility of the order of 1% with respect to the null hypothesis, for many on-source segments. Considering the γ factor, the parameter probing into the GW emission efficiency, we obtain $\sim 10^7$ and $\sim 10^3$, implying that the measure results are yet far away from the expected level under theoretical hypotheses. Therefore, the use of statistical arguments alone is not sufficient for deducing a systematic association between the two phenomena, but the study can turn out useful for further investigations. More observations are necessary in the direction of these intense sources. From this point of view, the recent improvements in gamma-astronomy are very encouraging. Over the last few years, various other important detectors have been launched, such as the AGILE mission [36] and Fermi Gamma-ray Space Telescope [37]. Other magnetars were also detected, such as the SGR 0501+4516 [38], the SGR 0418+5729 [39], and the very recent SGR 1833-0832 [40]. Thus, a fair amount of solid evidence exists for a more definite scientific strategy, studying multimessenger phenomena.

ACKNOWLEDGMENTS

We gratefully acknowledge the ROG collaboration for having made available the data of the GW detectors, and for the useful discussions.

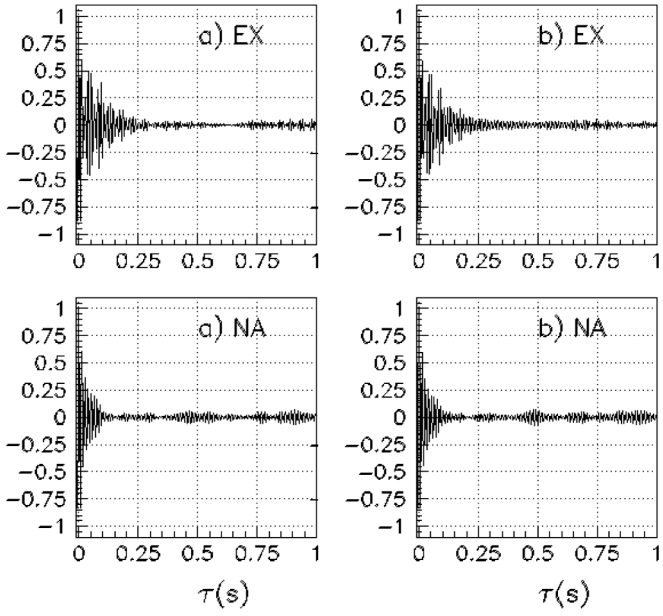

FIG. 4. Autocorrelation functions for both EXPLORER (up) and NAUTILUS (down) data. The checks are performed using 50s overlapping the on-source periods *a* and *b* (respectively on the left and on the right of the figure) both belonging to the October 5th outburst.

APPENDIX

1. Autocorrelation test

Performing the GW data analysis, three time intervals are chosen, as explained in Sec. III. The first two periods are each a few seconds long, but they have been divided into 1s segments for the analysis. To check the presence of local noise structures, as little glitch sequences or long bumps, that could invalidate the measurement also from the statistical point of view, we evaluated the autocorrelation function to the EXPLORER and NAUTILUS data of the on-source *a* and *b* periods chosen in the Sec. III. The result is shown in the Fig. 4. Although the checks are performed using 50s of data for each period, the graphics are presented up to 1s of time shift τ, given that the autocorrelation function drops within $\sim$200 ms, as we easily note, and the same behaviors continue on the whole periods.

2. Cosmic rays detection

The test validity is performed employing the real signals generated by extensive air showers (EASs) [23], and the filtered data of EXPLORER and NAUTILUS, all relative to the year 2004 [21,28]. Two events were selected, each for the single detector, with highest interaction energy with relative bar, in order to be independent of the noise. The responses of the two detectors are shown in Fig. 5. The selected EASs have, respectively, 3561 and 3128 of

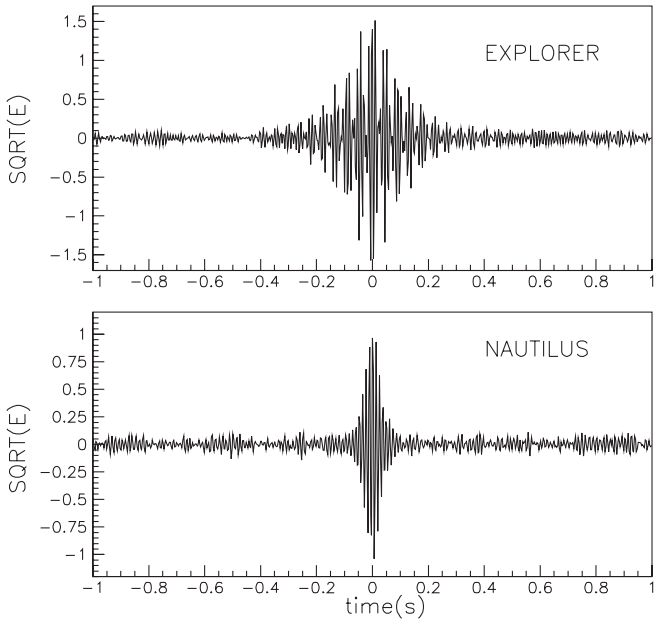

FIG. 5. Two selected cosmic ray showers producing in the two detectors signals much larger than noise. On the ordinate axis we show the $\sqrt{E}$, with the energy E in kelvin units. We notice the different resonance frequencies in the two detectors. The time of the two signals are shifted to an arbitrary *zero*, in order to simulate two simultaneous signals.

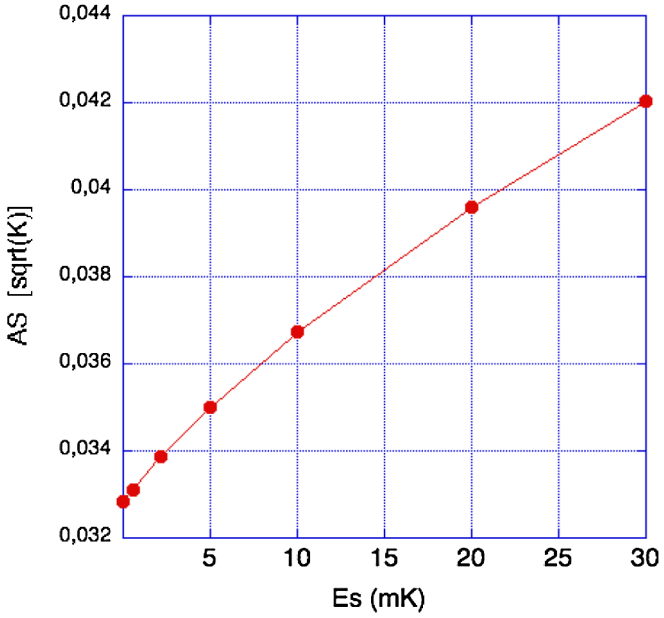

FIG. 6 (color online). The *AS* response, in squared *kelvin* units, versus the energy of cosmic ray calibration signals. For each point, 300 off-source measurements have been employed and averaged. At $E_s = 0$, the AS_{bck} value is reported. The continuous line is a polynomial fit.

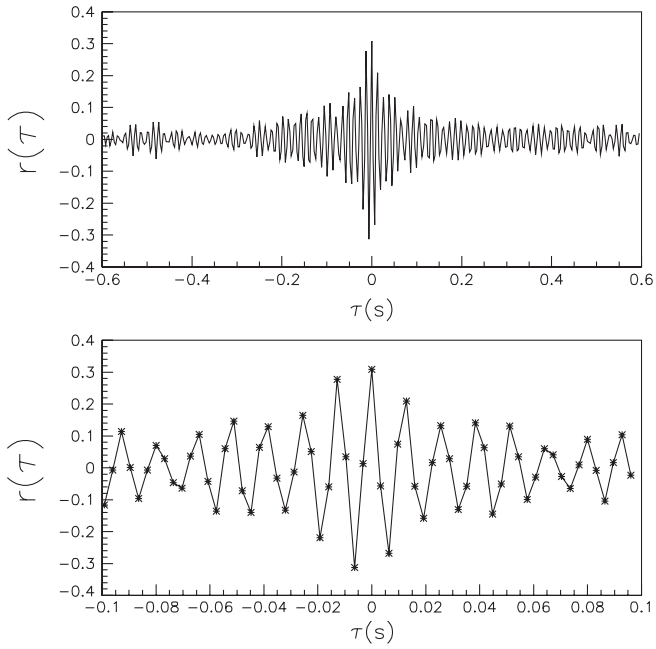

FIG. 7. The correlation function of the signals shown in the previous Fig. 5, versus the time shift. The *zero* on the abscissa is arbitrary.

particle multiplicity measured in the lower part of the cosmic ray detectors. The vibrational energy peaks are correspondently 2.47 K and 1.08 K, several hundred times the background, indicating a total energy of the order of 10 TeV deposited in each bar [23].

3. Average algorithm calibration

We use the typical envelope (see Fig. 5) for simulating deltalike signals. Obviously, we opportunely reduce each signal by scale factor depending on the choice of the amplitude signal. Then, we add the constructed signal-to the center time of 300x2 off-source regions using 10% of the background employed in the Sec. III B. In terms of energy, amplitude six values are chosen in the range 0.5–30 mK, and for each level, the average algorithm is applied obtaining the corresponding *AS* responses applying the Eq. (5). The calibration curve is reported in the Fig. 6. At $E_s = 0$, the AS_{bck} value is reported, as calculated in Sec. IV.

4. Cross-correlation response

To study the cross-correlation response, we use the EASs selected before and the corresponding GW data stretches showed in Fig. 5. The relative cross-correlation function is shown in Fig. 7. We note the oscillating behavior of the maximum response envelope in the temporal shift window of a few ten-milliseconds at zero time shift. This can compromise the efficiency of the cross-correlation detection algorithm, especially in very low signal-to noise-ratio conditions. To counter this, we adopt the r_{max} parameter, the maximum modulus of the cross-correlation function in the interval of ± 16 ms around the zero shift.

[1] E. P. Mazets, S. V. Golenetskii, V. N. Ilinskii *et al.*, Nature (London) **282**, 587 (1979).
[2] D. J. Helfand and K. S. Long, Nature (London) **282**, 589 (1979).
[3] R. C. Duncan and C. Thompson, Astrophys. J. **392**, L9 (1992).
[4] C. Thompson and R. C. Duncan, Astrophys. J. **473**, 322 (1996).
[5] T. Cline, E. Mazets, and S. V. Golenetskii, IAU Circ. **7002** (1998).
[6] S. Mereghetti, D. Gotz, A. von Kienlin *et al.*, Astrophys. J. **624**, L105 (2005).
[7] K. Hurley, S. E. Boggs, D. M. Smith *et al.*, Nature (London) **434**, 1098 (2005).
[8] S. Mereghetti, Astron. Astrophys. Rev. **15**, 225 (2008).

[9] J. A. de Freitas Pacheco, Astron. Astrophys. **336**, 397 (1998).
[10] K. Ioka, Mon. Not. R. Astron. Soc. **327**, 639 (2001).
[11] B. J. Owen, Phys. Rev. Lett. **95**, 211101 (2005).
[12] J. E. Horvarth, Mod. Phys. Lett. A **20**, 2799 (2005).
[13] C. J. Horowitz and K. Kadau, Phys. Rev. Lett. **102**, 191102 (2009).
[14] L. Baggio *et al.*, Phys. Rev. Lett. **95**, 081103 (2005).
[15] B. Abbott *et al.* (LIGO Scientic Collaboration), Phys. Rev. D **76**, 062003 (2007).
[16] G. L. Israel, T. Belloni, L. Stella *et al.*, Astrophys. J. Lett. **628**, L53 (2005).
[17] A. L. Watts and T. E. Strohmayer, Astrophys. J. Lett. **637**, L117 (2006).
[18] B. Abbott *et al.* (LIGO Scientic Collaboration) Phys. Rev. Lett. **101**, 211102 (2008).
[19] B. Abbott *et al.* (LIGO Scientic Collaboration), Astrophys. J. **701**, L68 (2009).
[20] P. Kalmus, K. C. Cannon, S. Marka, and B. J. Owen, Phys. Rev. D **80**, 042001 (2009).
[21] P. Astone *et al.* (ROG Collaboration) Classical Quantum Gravity **23**, S57 (2006).
[22] D. Gotz *et al.*, Astron. Astrophys. **445**, 313 (2006).
[23] P. Astone *et al.*, Astropart. Phys. **30**, 200 (2008).
[24] P. Astone *et al.* (ROG Collaboration), Phys. Rev. D **66**, 102002 (2002).
[25] P. Astone *et al.* (ROG Collaboration), Phys. Rev. D **71**, 042001 (2005).
[26] B. Abbott *et al.* (LIGO Scientic Collaboration), Phys. Rev. D **77**, 062004 (2008).
[27] B. Abbott *et al.* (LIGO & Virgo Collaboration), Astrophys. J. **715**, 1438 (2010).
[28] http://www.lnf.infn.it/esperimenti/rog/pub/dati.htm.
[29] P. Astone, C. Buttiglione, S. Frasca, G. V. Pallottino, and G. Pizzella, Nuovo Cimento Soc. Ital. Fis. **C20**, 9 (1997).
[30] E. Amaldi *et al.*, Nuovo Cimento Soc. Ital. Fis. **C9**, 829 (1986).
[31] P. Astone *et al.*, Astropart. Phys. **7**, 231 (1997).
[32] S. DAntonio, A. Pai, and P. Astone, J. Phys. Conf. Ser. **32**, 192 (2006).
[33] A. Pai *et al.*, Classical Quantum Gravity **24**, 1457 (2007).
[34] P. Astone *et al.* (IGEC Collaboration) Phys. Rev. D **82**, 022003 (2010).
[35] G. J. Feldman and R. D. Cousins, Phys. Rev. D **57**, 3873 (1998).
[36] M. Tavani *et al.* (AGILE Collaboration) NIMA **588**, 52 (2008).
[37] Y. Kaneko *et al.*, Astrophys. J. **710**, 1335 (2010).
[38] S. D. Barthelmy *et al.*, GCN Report No. 8113 Circular, 2008, http://gcn.gsfc.nasa.gov.
[39] A. J. van der Horst *et al.*, GCN Report No. 9499 Circular, 2009, http://gcn.gsfc.nasa.gov.
[40] J. M. Gelbord, S. D. Barthelmy *et al.*, GCN Report No. 10526, 10528 Circulars, 2010, http://gcn.gsfc.nasa.gov.